Transgenic construction and functional miRNA analysis identify the role of miR-7 in prostate cancer suppression

Bin Xu (101011584@seu.edu.cn)
Affiliated Zhongda Hospital of Southeast University
Can Wang
Wenchao Li
Qiang Hu
Ninghan Feng
Medical College of Nantong University https://orcid.org/0000-0002-0892-6102
Chun hui Liu
Naipeng Shi
Shuqiu Chen
Ming Chen
Han Guan
Zonghao You

Article

Keywords:

Posted Date: July 1st, 2022

DOI: https://doi.org/10.21203/rs.3.rs-1770961/v1

Version of Record: A version of this preprint was published at Oncogene on September 10th, 2022. See the published version at https://doi.org/10.1038/s41388-022-02461-0.

Title:

Transgenic construction and functional miRNA analysis identify the role of miR-7 in prostate cancer suppression

Can Wang[1,2 *], Wenchao Li[1,2 *], Qiang Hu[1,2 *], Nihan Feng[3*], Chunhui Liu[1,2], Naipeng Shi[1,2], Shuqiu Chen[1,2], Ming Chen[1,2], Han Guan[4], Zonghao You[1,2], Bin Xu[1,2]

1 Department of Urology, Affiliated Zhongda Hospital of Southeast University, Nanjing, 210009, China.

2 Surgical Research Center, Institute of Urology, Medical School of Southeast University, Nanjing, 210009, China.

3 Department of Urology, Wuxi No.2 hospital, Nanjing Medical University, Wuxi,214002, China.

4 Department of Urology, The First Affiliated Hospital of Bengbu Medical College, Bengbu, 233004, China.

Correspondence to: Bin Xu, Department of Urology, Affiliated Zhongda Hospital of Southeast University, 87 Dingjia Qiao, Nanjing, Jiangsu Province,210009, People's Republic of China, E-mail: njxbseu@seu.edu.cn or Zonghao You, Department of Urology, Affiliated Zhongda Hospital of Southeast University, 87 Dingjia Qiao, Nanjing, Jiangsu Province,210009, People's Republic of China, E-mail: 101012899@seu.edu.cn or Han Guan, Department of Urology, the First Affiliated hospital of Bengbu Medical College, 287 Chang Huai Road, Bengbu, Anhui Province 233004, People's Republic of China-mail: gh668689@126.com or Ming Chen, Department of Urology, Affiliated Zhongda Hospital of Southeast University, 87 Dingjia Qiao, Nanjing, Jiangsu Province, 210009, People's Republic of China, E-mail:mingchen0712@seu.edu.cn.

*These authors contributed equally to this work.

The authors declare no potential conflicts of interest.

Significance

Prostate cancer (PCa) is a major threat of men's health worldwide, with 20% to 50% patients harboring *TP53* mutation. Non-coding RNAs, especially miRNAs, act as crucial regulators in tumor initiation and progression, including PCa. Exploring the leading cause of miRNA abnormal expression and the mechanism of miRNA in PCa tumorigenesis will help the design promising therapeutic approaches. We find that miR-7 is regulated by *TP53* gene and inhibits the acidic microenvironment required for tumor formation, thus impacting on histone lactylation. Importantly, *in vivo* assays demonstrate efficacy of miR-7 on p53-negative tumors, highlighting that miR-7 could be a promising target for development of miRNA-based therapeutics, especially for PCa patients with p53 mutations.

Abstract

Although miR-7 suppresses the initiation and metastasis in cancers, including prostate cancer (PCa), little is known about its efficacy in the treatment of malignancy *in vivo*, especially in transgenic mouse models. Herein, to demonstrate the safety of *in vivo* miR-7 gene editing and its suppressive efficacy on p53-negative tumors, for the first time, a miR-7^{+} transgenic mouse model was constructed and hybridized with the TRAMP mice, whereby p53 was inhibited. miR-7 downregulated the glycolysis of PCa through the HIF pathway, thereby remodeling the acidic tumor macroenvironment, affecting histone lactylation and increasing T cell infiltration. miR-7 suppressed the PCa malignant behavior in LNCaP cells, prostatic primary tumor cells, and mice xenograft models. Moreover, *in vivo* miR-7 treatment prolonged the survival of mice with PCa and generated synergistic protective effects with PD-1 blockade due to the re-inflamed immune microenvironment. Furthermore, p53 acted as a transcriptional factor upregulating miR-7 expression, and therefore, the sensitization effects of exogenous miR-7 expression on PCa chemotherapeutic efficacy were independent of the p53 status. In summary, our findings highlighted a novel role of miR-7 in PCa. We describe herein, a promising target for the development of miRNA-based therapeutics, especially for PCa patients carrying p53 mutations.

Acknowledge

The authors disclosed receipt of the following financial support for the research, authorship, and/or publication of this article. This work was supported by the National Natural Science Foundation of China (grant numbers 81672551, 81370849, 81872089 and 82102799), Natural Science Foundation of Jiangsu Province (grant number BK20210230), Key Research and Development Program of Jiangsu Province (grant number BE2019751), Jiangsu Provincial Medical Talent (grant number ZDRCA2016080), The Jiangsu Provincial Medical Innovation Team (grant number CXTDA2017025), Natural Science Basic Research Program of Shanxi (grant number 2021JQ-023), Doctor of Entrepreneurship and Innovation in Jiangsu Province (grant number JSSCBS20210138), The General Project of Medical Research of Jiangsu Health and Wellness Committee(grant number M2020049)

.

Introduction

Prostate cancer (PCa) is the most common malignant tumor among men and the second leading cause of cancer deaths worldwide [1, 2]. Although currently, androgen deprivation therapy (ADT) is the major treatment for PCa, most patients show progression to castration-resistant prostate cancer (CRPC) within two years of ADT failure, and this is the leading cause of death due to PCa[3]. Few agents have been approved and these significantly improve the prognoses of patients with metastatic CRPC. Although immunotherapy, including PD-1/PD-L1 pathway blockades, show satisfactory clinical efficacy in different tumor types, the benefits for PCa patients remain limited.

TP53 encoding the tumor suppressor protein p53, a guardian of the genome, harbors the highest mutation rate in human cancers, with the rate of more than 50% [4]. The wild-type *TP53* mutation has been identified as an indispensable prerequisite for cancer initiation and progression, including PCa, harboring 20% to 50% *TP53* mutations[5-8]. Evidence suggests that *TP53* mutations play an important role in PCa chemotherapy resistance, thus preventing several patients with advanced PCa from benefiting from this first-line treatment [9, 10]. However, directly targeting *TP53* mutations in tumor treatment due to the functional and structural complexity of p53 wild-type proteins under physiological conditions, remains largely unsuccessful [11, 12]. Therefore, there is an urgent need for a deeper understanding of the role of p53 in tumorigenesis and examining alternative anti-tumor strategies for patients carrying *TP53* mutations.

MicroRNAs (miRNAs), a subset of non-coding small RNA molecules of 21-25 nucleotides in length, regulate gene expression in several pathways [13]. miRNAs can bind to specific mRNAs and inhibit their expression or promote their degradation at the post-transcriptional level[14]. Since the influences left by altered miRNA expression on human tumorigenesis are well-defined and

98 therapeutic approaches based on their role have been previously highlighted, these are promising
99 targets for treating tumors. miR-7, one of the most studied miRNAs, is evolutionarily conserved
100 across most sequenced bilaterian species, including humans and mice. miR-7 suppresses initiation
101 and metastases by targeting different signaling pathways in cancers [15, 16]. Gao et al.[17] report
102 that miR-7 expression is downregulated in docetaxel-resistant PCa tissues and tumor cells. However,
103 the efficacy of miR-7 in the treatment of malignancies has not been verified experimentally, *in vivo*,
104 especially in transgenic mice models.
105 Herein, we constructed a miR-7^{+} transgenic mouse model by overexpressing miR-7. Minimal organ
106 development abnormality was observed in these mice, indicating the safety of miR-7 editing *in vivo*.
107 The prostate tumor was significantly suppressed when the transgenic adenocarcinoma of the mouse
108 prostate (TRAMP) model, wherein *TP53* was inhibited, was crossed with miR-7^{+} mice to generate
109 the TRAMP^{+}/miR-7^{+} mice. Further *in vitro* and *in vivo* experiments demonstrated the suppressive
110 role of miR-7 expression in both initiation and maintenance of PCa regardless of the p53 status.
111 Additionally, miR-7 could relieve the inhibitory effects of the acid microenvironment caused by
112 glycolysis upon T cell activation through HIF-1α gene expression and reduce histone lactylation,
113 thus promoting anti-PD-1 treatment efficacy. Collectively, our findings demonstrated that miR-7
114 has therapeutic potential as a target in PCa treatment, especially among patients carrying *TP53*
115 mutations.

116 **Materials and methods**

117 **Patient samples**

118 Formalin-fixed paraffin-embedded PCa tissue samples were obtained from patients who underwent
119 radical prostatectomy in Affiliated Zhongda Hospital of Southeast University between February

2020 and November 2021, and the pathological diagnoses were confirmed by at least two pathologists. All patients did not receive any other treatments when they accepted radical prostatectomy. Tissue microarrays (TMA) were constructed using punches measuring 0.6 mm in diameter from blocks that included the tumor center, normal tissues adjacent to the tumor and lymph node metastases. The study design was approved by the Ethics Committee of the Affiliated Zhongda Hospital of Southeast University.

Cell lines and PCa organoids culture

Human (LNCaP, PC3, and PC-3M) and mouse (RM-1) PCa cell lines were obtained from the American Type Culture Collection (ATCC, USA). Cells were cultured in RPMI 1640 (Gibco Thermo Fisher Scientific, USA) supplemented with 10% fetal bovine serum (FBS) (LONSERA, Uruguay) and 1% penicillin-streptomycin solution (Keygen, China). For organoid culture, the human PCa (HPCa) samples were obtained after receiving the written informed consent from the patients. Tumor samples were cut into small chunks, rinsed twice with cold phosphate buffer saline (PBS), and then digested in collagenase I (Gibco Life Technology, USA) and TrypLE express (Gibco Life Technology, USA) in a 1:2 ratio in a 15 ml conical centrifuge tube (Corning, USA). The incubation time of the specimens depended on the amount of tissue collected and ranged from 30 min to 90 min until the suspension of most cell clusters. After digestion, cells were cultured in Dulbecco's modified eagle medium (DMEM, Gibco Life technology, USA) supplemented with the following growth factors: EGF 5–50 ng/ml (X-Bio technology, China), R-spondin1 conditioned medium or 500 ng/ml recombinant R-spondin1 (X-Bio technology, China), Noggin conditioned medium or 100 ng/ml recombinant Noggin (X-Bio technology, China), and 200 nM TGF-β/Alk inhibitor A83-01 (X-Bio technology, China). Dihydrotestosterone (X-Bio technology, China) was

added at a concentration of 0.1-1 nM. Medium composition and primary cell extraction were obtained following a previously reported procedure[18]. All cell lines were authenticated and free of mycoplasma.

Oligonucleotide and lentivirus transfection

miR-7 mimics, negative control for miRNA (miR-NC), anti-miR-7 oligos (miR-7 inhibitor), and negative control anti-miRNA (anti-miR-NC) were designed and synthesized by GenePharma (Shanghai, China) based on the miRbase database. PIK3CD and p53 small interfering (si)RNAs, NC siRNA were provided by GenePharma (Shanghai, China). miR-7 lentivirus, pcDNA-PIK3CD, pcDNA-p53 were provided by GenePharma (Shanghai, China). Cell transfection was performed using Lipofectamine 2000 (Beyotime, China), following the manufacturer's protocol. Cells were collected 48 h-72 h after transfection for subsequent experiments. Sequences used are listed in Supplementary **Table S1**.

RNA extraction and quantitative real-time polymerase chain reaction (qRT-PCR) analysis

RNA extraction kit (Takara Kusatsu, Japan) was used to extract total RNA from the PCa cells, and Hiscript II First-Strand cDNA Synthesis Kit was used to synthesize complementary DNA (cDNA). Gene U6 was used as the endogenous control, and the experiments were conducted in triplicates. Primers sequences were chemically synthesized by SprinGen Biotech (Nanjing, China) and are listed in Supplementary **Table S2**.

Cell proliferation and colony formation assays

For the proliferation assay, 800 cells were seeded in 96-well plates for 24 h-96 h, and 10 μl Cell Counting Kit-8 (Keygen, China) solution was added per well. After 37°C incubation for 4 h, optical density (OD) at 450 nm was measured on a microplate reader (Bio-Tek, USA). For the colony

formation, cells were seeded in 6-well plates at a density of 1-2×10^3 cells/well and incubated for 10-12 days at 37°C in 5% CO_2. Next, cells were washed using PBS, fixed with 4% polyformaldehyde (Service bio, China) and stained with 300 μL 0.1% crystal violet solution (Keygen, China). Colonies containing >50 cells were counted using the ImageJ 2X software 2.1.4.7 (Rawak Software Inc, Germany).

Transwell assays

To evaluate cell migration and invasion, a 24-well Transwell chamber, with an 8 μm pore membrane (Corning LifeSciences, USA), was utilized for the transwell assays. PC3 cells were inoculated in a 24-well Transwell cell apical chamber containing matrix gel (BD Biosciences, USA) for evaluating invasion and gel-free for migration. The bottom and upper chambers contained RPMI medium and FBS-free medium, respectively. Cells that invaded the bottom chambers were fixed with 4% polyformaldehyde, stained with 0.1% crystal violet solution, counted, and photographed under a microscope.

Flow cytometric analyses for cell cycle and apoptosis

For cell cycle detection, transfected cells were fixed with 75% cold ethanol overnight at -20°C, followed by staining with propidium iodide (PI). FACS flow cytometer (BD Biosciences, USA) was used for cell cycle distributions analyzed. The Beyotime apoptosis detection kit (China) was used to detect cellular apoptosis. Transfected PCa cells were stained with Annexin V-FITC and PI for 15 min. Data analysis was performed using the CellQuest Pro software (BD Biosciences, USA).

Glucose consumption, lactate production, enzyme, and adenosine triphosphatase (ATP) assays

The glucose oxidase assay kit (Rsbio, China) and Lactate LD Assay Kit (Keygen, China) were utilized to examine glucose uptake and lactate production, respectively. NADPH, citrate, G6PD and

ATP were measured using an enzyme-linked immunosorbent assay kit (Biocalvin, China), according to the manufacturer's protocol.

Assays to estimate extracellular acidification and oxygen consumption rate assays

Seahorse XFe 96 Extracellular Flux Analyzer (Seahorse Bioscience, USA) was used to determine the extracellular acidification rate (ECAR, mpH/min) and cellular oxygen consumption rate (OCR, pmol/min). ECAR and OCR were measured using the Seahorse XF Glycolysis Stress Test Kit and Seahorse XF Cell Mito Stress Test Kit, respectively (Seahorse Bioscience, USA), following the manufacturer's protocols. Data were assessed using the Seahorse XF-96 Wave software.

RNA sequencing and bioinformatics analysis

Cells stably overexpressing miR-7 were established by LV-miR-7 infection and puromycin selection. RNA sequencing was performed by Beijing CapitalBio Corporation (Beijing, China). Briefly, a total of 2 μg RNA was extracted from LV-miR-7 or LV-NC expressing cells, respectively. Then, RNA-sequencing was performed on the Illumina-HiSeq4000 system. Gene enrichment set analysis (GSEA) was used to identify gene sets or pathways which were relevant to the miR-7 expression profile in cells (http://www.broadinstitute.org/gsea/index.jsp). Hallmark of gene sets was obtained from the Molecular Signatures Database on that website. Normalized enrichment score (NES) and false discovery rate (FDR) were used to analyze across the gene sets.

Luciferase reporter assays

In 24-well plates, 1×10^5 cells per well were seeded. Cells were transfected with luciferase reporters. Lipofectamine 2000 (Invitrogen, USA) was used to co-transfect the wild-type or mutant ENO2/DPYSL2/CAMKK2/PIK3CD 3′-UTR constructs, in combination with miR-7 mimics or miRNA-NC. For dual luciferase assay, we co-transfected 1×10^5 cells with wild-type or mutant miR-

7 promoter reporter plasmids (GeneChem), in combination with pcDNA-p53. After incubation for 48 h, the cells were harvested. The Dual-luciferase Reporter Assay System (Promega, USA) was used to analyse the luminescence, which was normalized against Renilla luciferase activity.

Chromatin IP (CHIP) assay

CHIP assay was performed using an EZ CHIP kit (Millipore, USA) following the manufacturer's protocols. The immunoprecipitated DNA was purified and quantified by qRT-PCR to measure the p53 binding levels, which were normalized agains 2% input. The primer sequences used in the CHIP assay are listed in Supplementary **Table S2**.

Western immunoblotting analysis

Total proteins were extracted from PCa cells, lysed using radioimmunoprecipitation assay (RIPA) (Keygen, China) buffer, and quantified by a bicinchoninic acid (BCA) assay (Keygen, China). Proteins analyzed by 10% SDS-PAGE and the gels with separated proteins were transferred onto polyvinylidene fluoride (PVDF) membranes. Subsequently, the BSA-blocked PVDF membranes were incubated with specific primary antibodies ENO2(CST 9536,1:1000), DPYSL2(CST 35672,1:1000), CAMKK2(CST 16810,1:1000), PIK3CD (Thermo Fisher MA5-26514,1:500), p53 (CST 2527,1:1000), HIF-1α (CST 36169, 1:1000), total H3 (CST 4499, 1:2000), PanKLa (PTM biolabs, PTM-1401， 1:1000), and GAPDH (Service bio GB11002, 1:3000) overnight at 4°C, followed by incubation with secondary antibodies for 1 h. Finally, the protein bands were visualized using an enhanced- chemiluminescence kit (vazyme, China). The primary antibodies used in this experiment are listed in Supplementary **Table S**3.

In situ hybridization (ISH) and immunohistochemical staining (IHC)

The microRNA ISH Buffer and Control Kit (Boster, China) was used for ISH. The double (5′-3′)

digoxigenin-labelled miR-7 probe, U6 probe, and microRNA ISH Optimization Kit from Boster were used to conduct ISH, following the manufacturer's protocol. IHC was performed using mouse anti-human ki-67 (Proteintech, 27309-1-AP;1:1000), mouse anti-human HIF-1α (Proteintech, 20960-1-AP;1:200), mouse anti-human CD4 (CST, 25229S; 1:50-1:200) and mouse anti-human CD8 (Abcam, ab209775, 1:2000). Based on the intensity score, the percentage of positive cells was multiplied to obtain final immunoreactivity scores (IRSs) for Ki-67^{+} cells.

Xenograft studies and bioluminescence imaging analysis

Subcutaneous models

BALB/c nude mice (male, 6 weeks old) were purchased from ALF Biotechnology Co., Ltd (Jiangsu, China). PC3 cells (5×10^{6}) transfected with LV-miR-7/ LV-miR-NC were subcutaneously injected into the outer flanks of the nude mice. Seven days later, tumor sizes were measured at 4-day intervals to calculate tumour volume. At the endpoint of the experiments, mice were sacrificed, and the tumours were weighed.

Lung metastasis model

RM-1 cells (4×10^{6}) transfected with LV-miR-7/ LV-miR-NC (n = 5) were intravenously injected into the tail vein of C57BL/6 mice (male, 6 weeks old). At the endpoint of the experiments (30 days after tail vein injection), these mice were sacrificed and their lungs were photographed and fixed with 4% paraformaldehyde.

Orthotopic model

PC-3M cells (5×10^{6}, with fluorescence) were transfected with the LV-miR-7 construc and injected into the dorsal prostate lobes of nude mice. Bioluminescence imaging was performed 5 min and 28 days after injection, respectively.

Vivo-jetprime-miR-7/miR-NC treatment in subcutaneous and metastasis models

A total of 5×10^6 PC3 cells were suspended in 100 μl PBS and inoculated subcutaneously into the right flanks of nude mice. After 24 days, the transplanted nude mice were randomly divided into two groups (n = 4). Subsequently, Vivo-jetprime -miR-7 (10 μg mimics in 20 μl jetprime reagent) or Vivo-jetprime -miR-NC (Polyplus Illkirch France) subcutaneous intratumoral injection (twice a week) was administered. Tumor volume (V) was monitored by measuring the length (L) and width (W) using a Vernier caliper and calculated using the formula $V = (L\times W^2) \times 0.5$.

RM-1 cells (4×10^5) were injected into the tail vein, following which the mice were randomly divided into two groups (n = 5), with each group receiving miR-7 tail vein injection of in-vivo-jetprime reagent (30 μg mimics in 20 μl jetprime reagent) or NC mimic (once a week). Intraperitoneal injection of 200 μg anti-CD279 (PD-1) was administered every 3 days, starting on day 5 after initiation of miR-7 jetprime tail vein injection. After feeding for 28 days, computed tomography (CT) scanning was performed to calculate metastatic seeds.

All experimental animals were purchased from ALF Biotechnology Co., LTD (Jiangsu, China).

miR-7$^+$ transgenic mice and the TRAMP$^+$ model

miR-7$^+$ transgenic mice were constructed by Alingfei Biotechnology Co., Ltd (Jiangsu, China) (Supplementary material 1), using the PiggyBac transposon technology. Briefly, the miR-7 cDNA sequence was inserted into the pCAG systemic promoter, and the pCAG-miR-7 element was constructed between the two inverted terminal repeat elements of the PiggyBac transposon system. The constructed transgenic vector and transposase cRNA were co-injected into the zygotes of mice by microinjection. The fertilized mice eggs after injection were transplanted into the embryos. The founder mice were identified and screened by qRT-PCR and used for subsequent experiments.

TRAMP$^+$ (C57BL/6, male, 6 weeks old) mice were obtained from the Jackson Laboratory (USA). They were housed and crossed with C57BL/6 WT in the Animal Experimental Center of ALF, and heterozygous TRAMP$^+$ males were used in these experiments. The miR-7$^+$+TRAMP$^+$ double-transgenic mice (miR-7$^+$/ TRAMP$^+$) were obtained by crossing TRAMP$^+$ and miR-7$^+$ transgenic mice. All animal experimental protocols were approved by the Ethics Committee of Zhongda Hospital Affiliated to Southeast University and conducted following the National Guidelines for the Health Use of Laboratory Animals. qRT-PCR and the RNA sequencing analyses for miR-7 transgenic mice and double transgenic mice are shown in the Supplementary Fig 1.

Statistical analysis

The original miRNA expression and clinical data for PCa from The Cancer Genome Atlas (TCGA; www.cancergenome.nih.gov) were reanalyzed to investigate the clinical relevance of miR-7 expression for the pathologic traits of patients. Statistical analyses were performed using the SPSS software version 22.0 (SPSS, USA). Independent Student's t-tests and analysis of variance (ANOVA) were used to compare between groups. Data are presented as mean and SD. $P < 0.05$ was considered statistically significant.

Results

miR-7 expression impairs p53 null PCa development and inflames the immune microenvironment

miR-7 is evolutionarily conserved in humans and mice (Supplemental Fig. 1A). Therefore, we constructed transgenic mice overexpressing miR-7 (miR-7$^+$ mice) to explore the influence of miR-7 *in vivo* (Fig. 1A). Enhanced miR-7 expression was verified by qRT-PCR in the tail samples from 17-week miR-7$^+$ mice (Supplemental Fig. 1B, $P<0.05$). Minimal morphological alterations or

296 changes in weights of major organs including the prostate were observed in miR-7^{+} mice of different
297 ages (Fig. 1B, Supplemental Fig. 1C); similar ki67 expression (44.13%±2.37 in WT mice and
298 44.00%±3.39 in miR-7^{+} mice, P>0.05) was observed between miR-7^{+} or wild type (WT) mice
299 prostatic tissues (Fig. 1C), indicating the safety of *in-vivo* miR-7 gene editing. However,
300 subcutaneous tumors generated by injection of RM-1 cells in the flank of miR-7^{+} mice grew
301 significantly slower as compared to the wild-type mice, and the average size (P=0.04) and weight
302 (P<0.05) of xenografted tumors reduced significantly in the miR-7^{+} group (Supplemental Fig. 1D-
303 F).
304 Next, to verify the influence of miR-7 expression on PCa initiation and progression, transgenic
305 adenocarcinoma of the mouse prostate (TRAMP) model, typically employed for studying PCa
306 progression with inhibition of RB and TP53, were crossed with miR-7^{+} mice to generate the
307 TRAMP^{+}/miR-7^{+} line (Fig. 1A). TRAMP^{+}/miR-7^{+} mice at 15 weeks of age showed lower displayed
308 less prostatic intraepithelial neoplasia (PIN) ratio (39.00%±2.37 in TRAMP^{+} mice and 14.67%±2.08
309 in TRAMP^{+}/miR-7^{+} mice, P<0.05) and lower ki67 expression (13.67%±1.52 in TRAMP^{+} mice and
310 4.33%±0.58 in TRAMP^{+}/miR-7^{+} mice P=0.0006) than the correspondingly paired TRAMP^{+} mice
311 according to age, as evidenced by hematoxylin and eosin (HE) and immunohistochemistry (IHC)
312 staining assays (Fig. 1D-F). While at 20 weeks, a more obvious solid tumor formation was observed
313 in the prostate of TRAMP^{+} mice relative to the TRAMP^{+}/miR-7^{+} group (Fig. 1G). A significantly
314 higher PIN ratio (79.67%±4.73 in TRAMP^{+} mice and 18.33%±3.06 in TRAMP^{+}/miR-7^{+} mice,
315 P<0.05) was detected in TRAMP^{+} mice relative to the TRAMP^{+}/miR-7^{+} group (Fig. 1H).
316 Furthermore, TRAMP^{+}/miR-7^{+} mice showed a longer survival than TRAMP mice (Fig. 1M, n=8,
317 P<0.01), suggesting the *in-vivo* efficacy of miR-7 expression in suppressing PCa in p53 null mice.

PCa is an immunologically 'cold' tumor due to a low infiltration of T lymphocytes although androgen deprivation therapy (ADT) can promote T cell infiltration[19]. Herein, the tumor microenvironment in $TRAMP^+$/miR-7^+ mice tumor microenvironment showed an increased infiltration of $CD4^+$ (3.63%±0.70 in $TRAMP^+$ mice and 12.00%±0.56 in $TRAMP^+$/miR-7^+ mice $P<0.05$) and $CD8^+$ (2.77%±0.72 in $TRAMP^+$ mice and 14.50%±0.89 in $TRAMP^+$/miR-7^+ mice $P<0.05$) T cells and lower HIF-1α expression (29.70%±1.54 in $TRAMP^+$ mice and 8.33%±1.10 in $TRAMP^+$/miR-7^+ mice, $P<0.05$) as compared to the TRAMP mice (Fig. 1I-L), indicating greater immune microenvironment inflammation in PCa, which was moderated by miR-7. Taken together, these results demonstrated that the miR-7 has a prominent role in impairing p53 null PCa tumorigenesis and remodeling the tumor microenvironment of PCa.

miR-7 inhibits glycolysis in prostate cancer cells through the HIF-1α pathway

Previous results showed the effects of miR-7 on PCa suppression, thus we further examined the target genes and downstream pathways of miR-7. RNA sequencing for miR-7 overexpressing PCa cells as compared to miR-NC cells followed by GO analysis and GSEA showed negative enrichment of metabolism-related pathways including, glycolysis and the HIF-1α signaling pathway (Fig. 2A). HIF-1α, which can be stabilized in a hypoxia tumor microenvironment, can regulate a cluster of glycolytic genes, including HK2, PKM2, and LDHA[20-22]. Herein, we confirmed that HK2, PKM2 and other glycolysis rate-limiting enzymes in glycolysis were downregulated after miR-7 was overexpressed in LNCaP cells (Fig. 2B).

To verify the role of miR-7 expression in glycolysis, LNCaP cells were firstly transfected using miR-7 mimics and inhibitors. The transfection efficiency in PCa cells is shown in Supplementary Fig. 3A-B. We found that miR-7 mimics decreased extracellular acidification rate (ECAR) and

increased the oxygen consumption rate (OCR), thereby suppressing the Warburg effect (Fig. 2C, D). miR-7 mimics significantly reduced glucose consumption, lactate production, and ATP content in cancer cells, whereas the miR-7 inhibitor significantly enhanced these glycolytic processes (Fig. 2E-G, Supplementary Fig. 3J-L). Furthermore, miR-7 inhibited the expression of key enzymes in glucose metabolism, including G6PD, NADPH, and CITRATE in LNCaP and PC3 cells (Supplementary Fig. 3G-I). The effects of miR-7 on cellular proliferation in the presence of two metabolic inhibitors, glycolysis inhibitor 2-DG and ATP synthase inhibitor oligomycin, were examined. The results revealed differences in the cell proliferation between miR-7 overexpressing LNCaP cells and control cells, which were reduced in a 2-DG dose-dependent manner. Consistently, LNCaP cells overexpressing miR-7 were less sensitive to the glycolysis inhibitor, 2-DG, as compared to the control group (Supplementary Fig. 1M, N, O and P).

To further examine the downstream targets of miR-7, eight genes were likely to be regulated by miR-7 based on the overlap in the results from Targetscan, miRDB, and the microarray for PC3 and LNCaP cells. Among these genes, PIK3CD, CAMKK2, DPYSL2, and ENO2 reportedly participated in the process of glycolysis, and their involved pathways were all upregulated or directly targeted by HIF-1α[23-28]. Herein, we also confirmed downregulated expression by miR-7 through western blotting (Fig. 2H, I). Additionally, a stably high HIF-1α and PanKLa (Histone pan lysine lactylation) expression under cobalt chloride conditions were also detected in the miR-NC PCa cells as compared to the miR-7 group (Fig. 2I). Luciferase reporter gene assays showed that miR-7 directly inhibited the transcriptional activity of PIK3CD, CAMKK2, DPYSL2 and ENO2 by binding to their promoter regions (Fig. 2J-M). As PIK3CD is a crucial member in the classic PI3K/AKT/HIF-1α axis regulating tumor metabolism and that glycolysis is regulated by

362 miR-7, we next examined whether miR-7's effects on PCa cell glucose metabolism were regulated
363 by it. LNCaP cells treated with PIK3CD siRNA or PI3K/AKT pathway inhibitor, LY294002,
364 showed significantly reduced glucose consumption, lactate production, and proliferation
365 (Supplemental Fig. 2). PIK3CD could reverse the suppressed proliferation, colony formation, and
366 glycolysis in LNCaP cells through miR-7 (Supplemental Fig. 3C-F). Collectively, these results
367 indicated the suppressive role of miR-7 on HIF-1α, thereby downregulating the glycolysis process
368 in prostate cells.

369 **miR-7 suppresses PCa cell proliferation and tumorigenesis**

370 Next, *in vitro* experiments were performed to examine the effects of miR-7 expression on the
371 malignant behavior of PCa cells. LNCaP cells were transfected with vectors to overexpress or knock
372 down miR-7, and these corresponding changes were verified by qRT-PCR (Supplementary Fig. 3A).
373 The proliferation and colony formation abilities of malignant cells were attenuated upon miR-7
374 overexpression but enhanced upon miR-7 knockdown (Fig. 3A, B). Moreover, miR-7
375 overexpression induced cells apoptosis (Fig. 3C) and blocked cell cycle progression (Fig. 3D).
376 Although miR-7 expression was negatively associated with the malignant behavior in PCa cell lines,
377 some studies on primary human prostate cancer (HPCa) cells have been reported. To evaluate the
378 biological functions of miR-7 in PCa primary cells and organoids, tumour specimens were quickly
379 processed and epithelial HPCa cells were purified，transfected with miR-7 or NC oligos. HPCa
380 cells overexpressing miR-7 showed reduced glucose consumption, lactate production, impaired cell
381 proliferation, and colony formation capacities (Fig. 3E-H). Strikingly, the PCa organoids' average
382 radii and area in the miR-7 transfection group were smaller relative to the miR-NC transfection
383 group (Fig. 3I), indicating that miR-7 also manifested its inhibitory effects in primary PCa cells.

Collectively, we demonstrated that miR-7 negatively regulated the malignant behavior of PCa cells. Next, subcutaneous xenografts were used to confirm the suppressive effects of miR-7 on PCa *in vivo*. miR-7-overexpressing PC3 cells were subcutaneously injected, and the tumor sizes and weights were recorded. The results showed a reduction in the average size ($P<0.05$) and weight ($P< 0.05$) of the tumor xenografts in the miR-7 overexpression group as compared to the control group (Fig. 3J-L). Moreover, $ki67^+$ expression was suppressed in lentivirus-miR-7 treated tumours (Fig. 3M, 12.8%±2.26 in lentivirus-miR-NC treated cells and 4.00%±1.31 in in lentivirus-miR-7 treated cells, $P=0.0043$). Subsequently, luciferase-labelled LV-miR-7 or LV-miR- NC vector-transfected PC-3M cells were inoculated into the dorsal prostate lobes of male nude mice (Fig. 3N). After 28 days, bioluminescence imaging showed that the signal intensity in the miR-7 overexpression group was weaker relative to the control vector group (Fig. 3O, $1.61\times10^6\pm0.38\times10^6$ in luciferase-labelled LV-miR-NC treated cells and $0.02\times10^6\pm0.04\times10^6$ in luciferase-labelled LV-miR-NC treated cells, $P< 0.05$), suggesting that miR-7 transfection inhibited PCa formation *in vivo*. As miR-7 is evolutionarily conserved between humans and mice, a metastatic model was constructed using murine PCa cells, RM-1, which possesses the favorable metastatic ability (Fig. 3P). The tail vein injection of LV-miR-7 treated RM-1 cells resulted in a significant reduction in metastatic seeding and growth in explanted lungs as compared to the LV-miR-NC vector group, which was confirmed through pathological screening of pulmonary specimens (Fig. 3Q, R).

Therapeutic effects of miR-7 in mouse prostate cancer and lung metastasis

Given the pivotal role of miRNAs in tumor initiation and progression, these non-protein-coding RNAs are potential cancer biomarkers and therapeutics targets[29, 30]. To examine the therapeutic potential of miR-7 in PCa, the tumour-inhibitory effects of miR-7 in a xenograft model were

406 evaluated. PC3 cells (5×10^6 cells/40μl) were subcutaneously implanted in BALB/c mice. On day 14,
407 mice with approximately 100 mm^3 tumor volumes were randomly divided into two subgroups, with
408 each group either receiving an intra-tumor injection of either miR-7-jetprime agent or NC mimics
409 (Fig. 4A). The results showed that miR-7 injection slowed down tumor growth, and the tumor
410 volume ($P<0.05$) and weight ($P<0.05$) decreased significantly after 6 injections of miR-7-jetprime
411 as compared to the NC mimics injection group (Fig. 4B-D). IHC staining in the harvested tumor
412 specimens revealed a reduction in the ki67 expression in the miR-7-jetprime injection group (Fig.
413 4E,14.30±3.18 in miR-NC-jetprime injection group and 4.50%±1.77 in miR-7-jetprime injection
414 group, P=0.0017). Additionally, the subcutaneously transplanted tumors in mice were treated by
415 wrapping miR-7 with Polys (β-amino ester) (PABE) nanomaterials (Supplementary Fig. 4A). The
416 growth of subcutaneous tumors in mice was inhibited after treatment by wrapping miR-7 with PABE
417 (Supplementary 4B-C).
418 Intriguingly, significantly higher CD4 (3.80%±0.26 in miR-NC-jetprime injection group and
419 11.80%±0.60 in miR-7-jetprime injection group, $P<0.05$) and CD8 (5.90%±0.79 in miR-NC-
420 jetprime injection group and 16.83%±0.40 in miR-7-jetprime injection group, $P<0.05$) positive
421 lymphocytes infiltration and lower HIF-1α expression (30.60%±3.34 in miR-NC-jetprime injection
422 group and 10.70%±1.78 in miR-7-jetprime injection group, $P<0.05$) were observed in miR-7-
423 jetprime-injected tumors (Fig. 4F-I). Considering the previously demonstrated role of miR-7 on the
424 tumor metabolic pathway, these results indicated that miR-7 inhibited glycolysis through the HIF
425 pathway, thereby moderating the acidic tumor microenvironment and creating favorable conditions
426 for anti-tumoral immune cell infiltration. Infiltration of T cells, which are recognized anti-tumor
427 effectors, is directly related to enhanced efficacy of anti-PD-1 therapy for tumors[31]. Therefore,

the tail vein pulmonary metastasis model was used to investigate the therapeutic potential of miR-7, as well as that in combination with anti-PD-1 therapy. Mice were randomly divided into three subgroups after injection of RM-1 cells into the tail vein (80μl PBS containing 4×10^5 cells). Tail vein injection treatment with miR-7/NC-jetprime reagent (once a week) or combined with PD-1 blockade (every 3 days) was administered. After feeding for 28 days, mice were anesthetized to obtain the CT scans, wherein jetprime-miR-7 was found to significantly reduce the metastatic seeding in the explanted lungs as compared to that in the jetprime-miR-NC group (Fig. 4J, K). The result was validated by HE staining in the harvested lungs (Fig. 4L, M). Overall survival analysis revealed that mice in the jetprime-miR-7 group survived longer than the jetprime-miR-NC group, indicating the therapeutic potential of miR-7 in PCa (Fig. 4N). Additionally, when combined with anti-PD-1 therapy, miR-7-jetprime showed the most significant therapeutic efficacy and the best survival outcome among all the three examined groups($P<0.01$). In summary, we demonstrated the therapeutic effects of miR-7 in mouse prostate cancer and lung metastasis, along with its significant synergy with anti-PD-1 therapy.

The tumor suppressor, *TP53,* transcriptionally upregulates miR-7

TP53 modulates miRNA expression as a transcription factor[32, 33], and the genomic location analysis for p53 showed its location upstream of the pri-miR-7 sequence (Fig. 5A). To identify the role of p53 in miR-7 transcription, the effects of abnormal p53 levels on miR-7 expression were analyzed. The qRT-PCR results showed that p53 overexpression led to the increased miR-7 expression, whereas downregulation of p53 led to decreased miR-7 expression (Fig. 5B, C). The transfection efficiency was verified by western blot assay (Supplemental Fig. 4D, E). To confirm the regulatory role of p53 on miR-7 transcription, p53 binding sites in the promoter region of pri-

miR-7 were predicted using the Jaspar software (Fig. 5D). Reporter plasmid vectors contained the WT or MUT seed sequences of p53 binding sites in the promoter region of pri-miR-7 (-806bp to -823bp and -832bp to -849bp). The luciferase activity of the WT vector for the binding sites increased as compared to the MUT vector (Fig. 5E). Additionally, CHIP assays demonstrated that chromatin fragments containing putative p53 binding sequences were specifically present in anti-p53 immunoprecipitated cells (Fig. 5F). Therefore, based on the luciferase and CHIP assays, p53 could potentially bind directly to the promoter region, thus upregulating miR-7 transcription.

Doxorubicin (Dox), which can promote the expression of p53, is an efficient chemotherapeutic agent that is widely used in the treatment of various cancer types[34]. LNCaP cells (p53 WT) and PC3 cells (p53 null) were treated with Dox to elucidate the different responses of cells. LNCaP cells (p53 WT) and PC3 cells (p53 null) were treated with Dox to elucidate the differential responses of these cells. The half maximal inhibitory concentration (IC50) in PC3 cells was higher relative to the LNCaP cells (Fig. 5G, K), indicating that drug resistance persisted longer in p53 null cells as compared to the p53 WT cells. As chemoresistance is a major cause of cancer recurrence, the potential of miR-7, which is regulated by p53, to reverse cellular resistance to Dox treatment was further examined. p53 and miR-7 expressions were augmented with increasing Dox treatment in LNCaP cells (Fig. 5H, I, Supplementary Fig. 4F), and miR-7 could enhance the sensitivity of p53 WT cells to Dox, which was confirmed by LNCaP cellular apoptosis and IC50 assays (Fig. 5J). Furthermore, miR-7 overexpression increased the sensitivity to Dox even in the p53 null PCa cell line (Fig. 5K) although Dox itself did not influence the expression of miR-7 or p53 (Fig. 5L, Supplemental Fig. 4G), thus indicating miR-7 could potentially reverse p53 mutation-induced cell resistance to chemotherapy.

Database analysis for miR-7 and *TP53* expression in prostate cancer

The PCa specimens collected in Affiliated Zhongda Hospital of Southeast University showed lower miR-7 expression in tumor tissues as compared to the adjacent normal tissues (Supplemental Fig. 4J), which was validated by the ISH assay in large sections and tissue microarray (Fig. 6A, B). Furthermore, a significant negative correlation was observed in PCa patients between the ISH score and SUVmax obtained from PET-CT (Fig. 6C). miR-7 and p53 levels in the PCa normal and tumor tissues and their correlation with clinical outcomes were further analyzed based on TCGA database. The results showed that p53 expression was downregulated in PCa as compared to normal tissues (Supplementary Fig. 4H), and patients with higher p53 expression (PCa patients were divided into high/low groups according to the median expression of p53) or with wild-type p53 status showed a longer overall survival (Fig. 6D, E, Supplementary Fig. 4I). Additionally, the expression of miR-7 was downregulated in PCa patients with TP53 mutations (Fig. 6F), and those with higher expression of miR-7 (PCa patients were divided into high/low groups according to the median expression of miR-7) survived longer relative to patients with low miR-7 expression (Fig. 6G). In summary, the above results demonstrated that miR-7 was up-regulated by TP53, and exogenous miR-7 could exert favorable anti-tumor effects even in the absence of p53.

Discussion

In recent years, the in-depth understanding of the miRNAs' roles has made them attractive tools and targets for designing novel therapies[35]. Several therapeutic targeted miRNAs have undergone/are at different stages of clinical trials, including phase I clinical trials for treating cancer using a mimic of miR-34[36], phase II trials for treating hepatitis targeted at miR-122[37], and those for treating mesothelioma utilizing miR-16-based mimic drug[38]. miRNA-based anti-cancer strategies hold

great promise for cancer treatment, especially those showing limited efficacy with conventional therapies. miR-7, which is one of the most studied miRNAs, reportedly suppresses tumor progression through multiple fundamental biological processes by affecting various signaling pathways[39-42]. In prostate cancer, miR-7 inhibits tumor cell stemness and tumorigenesis through the KLF4/PI3K/Akt signaling axis[43]. Activation of miR-7 increases the chemotherapeutic sensitivity of prostate cancer[17]. Previous studies indicate the therapeutic potential of miR-7 in tumors. However, currently, there is a lack of animal models to further determine the safety and efficacy of miR-7 for tumor therapies. Herein, for the first time, we constructed miR-7 overexpressing transgenic mice (miR-7^{+} mice), whereby no significant abnormality in organ development or acceleration of cell proliferation was observed, thus indicating the safety of *in-vivo* miR-7 gene editing. Moreover, *in-vivo* tumorigenesis experiments utilizing miR-7 overexpressing prostate cancer cells and miR-7-jetprime in mice model validated the tumor suppressive effects of miR-7 in the progression and metastasis of prostate cancer.

In addition, through *in-vitro* experiments, we demonstrated that p53 could transcriptionally upregulate miR-7 expression by binding to its promoter region. *TP53* is a key tumor suppressor in the development of various cancers, and its missense mutations could ruin the specific DNA binding activity or cause misfolding, thereby promoting cancer initiation and progression[44]. Understanding how *TP53* signaling leads to changes in gene expression, ultimately resulting in tumorigenesis is of paramount importance for the development of effective therapeutic strategies. The TRAMP murine model, wherein *TP53* is inhibited, spontaneously produces prostatic tumor[45]. It is a typical model for studying PCa progression. Herein, we hybridized the miR-7^{+} mice with $TRAMP^{+}$ mice, and observed a significantly reduction in tumor volume and prolonged survival in

516 TRAMP^{+}/miR-7^{+} mice. Furthermore, in p53 wild-type prostate cancer cells (LNCaP), a significant
517 cellular response to a DNA-damaging chemotherapeutic drug, Dox, was observed. Dox is a
518 commonly used effective agent for PCa patients, which is known to induce apoptosis in malignant
519 cells[46]. PCa patients carrying *TP53* mutations lack sensitivity to Dox treatment, thus indicating
520 that p53 is required for Dox-induced apoptosis[47, 48]. However, in our study, p53-induced
521 apoptosis of tumor cells showed a remarkable reduction upon miR-7 inhibition. These results proved
522 that miR-7 expression was upregulated by p53, and the cellular function of the latter was also
523 significantly suppressed in the absence of the former.
524 According to multiple previous studies, *TP53* activated mutations are present in a large fraction of
525 human tumors including PCa, and this ratio in lethal metastasis castration-resistant PCa (mCRPC);
526 it ranges from 30% to 70%, which is significantly higher relative to primary PCa[49-52]. The
527 frequent mutation rate of *TP53* and its close association with tumorigenesis make it an attractive
528 target for developing anti-tumor strategies. However, it is extremely difficult to singly target the
529 *TP53* mutation without disturbing the complex biological functions and structures of the wild-type
530 p53 protein[53]. Herein, we found that the sensitivity to Dox therapy was significantly lower in p53
531 null cell lines (PC3) relative to p53 wild-type LNCaP cells, wherein low p53 expression was
532 validated in PC3 cells by western blotting assay under either Dox or DMSO condition. However,
533 miR-7 re-sensitized the PC3 cells to Dox treatment. Moreover, as discussed previously, prostate
534 cancer initiation was promoted in p53-suppressed TRAMP+ transgenic mice, whereas
535 tumorigenesis progression was significantly reversed upon overexpression of miR-7 in TRAMP+
536 mice. Collectively, these results convincingly demonstrated that miR-7, a downstream factor of p53,
537 preserved a favorable anti-tumor activity even upon p53 deficiency.

Glucose metabolism is the key source of metabolic carbon for cancer cells, even in the presence of ample oxygen[54]. In the present study, RNA sequencing analysis of PCa cells revealed that the metabolic pathways, especially HIF-1α signaling and glycolysis, were significantly enriched in miR-7 overexpressing tumor cells. We then validated *in-vitro* that miR-7 inhibited glycolysis by targeting HIF-1α signaling, thereby reducing glucose consumption and lactate production in malignant cells. HIF-1α is a classic transcription factor that exists widely in mammals and humans under hypoxic conditions and produces an acidic tumor microenvironment[55]. Lactate accumulation by glycolysis is also a crucial factor causing a decrease in pH in the microenvironment, thus promoting tumor immune escape[56]. Histone lactylation, the newly identified epigenetic modification regulated by lactate accumulation, was shown to mediate the transcriptional of certain genes associated with restoration of macrophage transformation[57-59]. Intriguingly, in this study, ectopic miR-7 expression decreased lactate production and led to reduced PanKLa expression, which suppressed PCa cell malignant behavior at last. This phenomenon interestingly demonstrated that the suppressor role of miR-7 could be due to its effect on histone lactylation, which is influenced by lactate production. Furthermore, HIF is directly involved in the regulation of the PD-1/PD-L1 pathway, suggesting the therapeutic potential of combining HIF and immune checkpoint inhibitors (ICIs). ICIs have emerged as a durable therapeutic option for some specific tumor entities but PCa, a typical “cold” tumor, which is characterized by a lack of anti-tumor T lymphocytes, shows minimal benefit from this promising treatment strategy[60]. Herein, in the $TRAMP^{+}$/miR-7^{+} transgenic mice, we found that miR-7 not only inhibited the expression of HIF1a, but also promoted the tumoral infiltration of $CD4^{+}$ T helper cells and $CD8^{+}$ cytotoxic T lymphocytes. Furthermore, the combination of miR-7-jetprime with PD-1 blockade significantly delayed the formation of lung

metastasis and prolonged the survival of PCa mice. Collectively, these findings not only revealed the mechanism underlying miR-7 action for suppressed tumorigenesis but also provided a basis for the synergistic potential of miR-7 and immunotherapy in PCa.

In summary, we show the safety and efficacy of miR-7 in p53-negative PCa treatment through multiple *in-vivo* transgenic mice models. Furthermore, miR-7 downregulated the glycolysis of PCa through the HIF pathway, thereby remodeling the acidic tumor macroenvironment, affecting histone lactylation and increasing T cell infiltration. In addition, p53 acted as a transcriptional factor upregulating miR-7 expression, and therefore, the sensitization effects of exogenous miR-7 expression on PCa chemotherapeutic efficacy were independent of the p53 status. With the development of miRNA-targeted drugs, we believe that miR-7 mimic-based agents could serve as a promising therapeutic option for PCa patients, especially those carrying *TP53* mutations.

Reference

1 Siegel RL, Miller KD, Fuchs HE, Jemal A. Cancer statistics, 2022. *CA Cancer J Clin* 2022; 72: 7-33.

2 Culp MB, Soerjomataram I, Efstathiou JA, Bray F, Jemal A. Recent Global Patterns in Prostate Cancer Incidence and Mortality Rates. *Eur Urol* 2020; 77: 38-52.

3 Sehrawat A, Gao L, Wang Y, Bankhead A, 3rd, McWeeney SK, King CJ *et al*. LSD1 activates a lethal prostate cancer gene network independently of its demethylase function. *Proc Natl Acad Sci U S A* 2018; 115: E4179-E4188.

4 Wang M, Attardi LD. A Balancing Act: p53 Activity from Tumor Suppression to Pathology and Therapeutic Implications. *Annu Rev Pathol* 2022; 17: 205-226.

5 Muller PA, Vousden KH. p53 mutations in cancer. *Nat Cell Biol* 2013; 15: 2-8.

6 Zhang C, Liu J, Xu D, Zhang T, Hu W, Feng Z. Gain-of-function mutant p53 in cancer progression and therapy. *J Mol Cell Biol* 2020; 12: 674-687.

7 Robinson D, Van Allen EM, Wu YM, Schultz N, Lonigro RJ, Mosquera JM *et al*. Integrative clinical genomics of advanced prostate cancer. *Cell* 2015; 161: 1215-1228.

8 Liu Z, Guo H, Zhu Y, Xia Y, Cui J, Shi K *et al*. TP53 alterations of hormone-naïve prostate cancer in the Chinese population. *Prostate Cancer Prostatic Dis* 2021; 24: 482-491.

9 Rucker FG, Schlenk RF, Bullinger L, Kayser S, Teleanu V, Kett H *et al*. TP53 alterations in acute myeloid leukemia with complex karyotype correlate with specific copy number alterations, monosomal karyotype, and dismal outcome. *Blood* 2012; 119: 2114-2121.

10 Liu C, Zhu Y, Lou W, Nadiminty N, Chen X, Zhou Q *et al*. Functional p53 determines docetaxel sensitivity in prostate cancer cells. *Prostate* 2013; 73: 418-427.

11 Bromley D, Daggett V. Tumorigenic p53 mutants undergo common structural disruptions including conversion to alpha-sheet structure. *Protein Sci* 2020; 29: 1983-1999.

12 Joerger AC, Fersht AR. Structural biology of the tumor suppressor p53 and cancer-associated mutants. *Adv Cancer Res* 2007; 97: 1-23.

13 Denli AM, Tops BB, Plasterk RH, Ketting RF, Hannon GJ. Processing of primary microRNAs by the Microprocessor complex. *Nature* 2004; 432: 231-235.

14 Shukla GC, Singh J, Barik S. MicroRNAs: Processing, Maturation, Target Recognition and Regulatory Functions. *Mol Cell Pharmacol* 2011; 3: 83-92.

15 Lin CL, Ying TH, Yang SF, Wang SW, Cheng SP, Lee JJ *et al*. Transcriptional Suppression of miR-7 by MTA2 Induces Sp1-Mediated KLK10 Expression and Metastasis of Cervical Cancer. *Mol Ther Nucleic Acids* 2020; 20: 699-710.

16 Pan CM, Chan KH, Chen CH, Jan CI, Liu MC, Lin CM *et al*. MicroRNA-7 targets T-Box 2 to inhibit epithelial-mesenchymal transition and invasiveness in glioblastoma multiforme. *Cancer Lett* 2020; 493: 133-142.

17 Gao Y, Liu J, Huan J, Che F. Downregulation of circular RNA hsa_circ_0000735 boosts prostate cancer sensitivity to docetaxel via sponging miR-7. *Cancer Cell Int* 2020; 20: 334.

18 Karthaus WR, Iaquinta PJ, Drost J, Gracanin A, van Boxtel R, Wongvipat J *et al*. Identification of multipotent luminal progenitor cells in human prostate organoid cultures. *Cell* 2014; 159: 163-175.

19 Qi Z, Xu Z, Zhang L, Zou Y, Li J, Yan W *et al*. Overcoming resistance to immune checkpoint therapy in PTEN-null prostate cancer by intermittent anti-PI3Kα/β/δ treatment. *Nat Commun* 2022; 13: 182.

20 Li Z, Peng Y, Li J, Chen Z, Chen F, Tu J *et al*. N(6)-methyladenosine regulates glycolysis of cancer cells through PDK4. *Nat Commun* 2020; 11: 2578.

21 Wang C, Li Y, Yan S, Wang H, Shao X, Xiao M *et al*. Interactome analysis reveals that lncRNA HULC promotes aerobic glycolysis through LDHA and PKM2. *Nat Commun* 2020; 11: 3162.

22 Ren R, Guo J, Shi J, Tian Y, Li M, Kang H. PKM2 regulates angiogenesis of VR-EPCs through modulating glycolysis, mitochondrial fission, and fusion. *J Cell Physiol* 2020; 235: 6204-6217.

23 Zhang T, Niu X, Liao L, Cho EA, Yang H. The contributions of HIF-target genes to tumor growth in RCC. *PLoS One* 2013; 8: e80544.

24 Westra J, Brouwer E, van Roosmalen IA, Doornbos-van der Meer B, van Leeuwen MA, Posthumus MD *et al*. Expression and regulation of HIF-1alpha in macrophages under inflammatory conditions; significant reduction of VEGF by CaMKII inhibitor. *BMC Musculoskelet Disord* 2010; 11: 61.

25 George AL, Rajoria S, Suriano R, Mittleman A, Tiwari RK. Hypoxia and estrogen are functionally equivalent in breast cancer-endothelial cell interdependence. *Mol Cancer* 2012; 11: 80.

26 Lee KS, Kim SR, Park SJ, Min KH, Lee KY, Choe YH *et al*. Mast cells can mediate vascular permeability through regulation of the PI3K-HIF-1alpha-VEGF axis. *Am J Respir Crit Care Med* 2008; 178: 787-797.

27 Riganti C, Doublier S, Viarisio D, Miraglia E, Pescarmona G, Ghigo D *et al*. Artemisinin induces doxorubicin resistance in human colon cancer cells via calcium-dependent activation of HIF-1alpha and P-glycoprotein overexpression. *Br J Pharmacol* 2009; 156: 1054-1066.

28 Cardozo V, Vaamonde L, Parodi-Talice A, Zuluaga MJ, Agrati D, Portela M *et al*. Multitarget neuroprotection by quercetin: Changes in gene expression in two perinatal asphyxia models. *Neurochem Int* 2021; 147: 105064.

29 Wang J, Chen J, Sen S. MicroRNA as Biomarkers and Diagnostics. *J Cell Physiol* 2016; 231: 25-30.

30 Sahraei M, Chaube B, Liu Y, Sun J, Kaplan A, Price NL *et al*. Suppressing miR-21 activity in tumor-associated macrophages promotes an antitumor immune response. *J Clin Invest* 2019; 129: 5518-5536.

31 Ribas A, Dummer R, Puzanov I, VanderWalde A, Andtbacka RHI, Michielin O *et al*. Oncolytic Virotherapy Promotes Intratumoral T Cell Infiltration and Improves Anti-PD-1 Immunotherapy. *Cell* 2017; 170: 1109-1119 e1110.

32 Bayraktar R, Ivan C, Bayraktar E, Kanlikilicer P, Kabil NN, Kahraman N *et al*. Dual Suppressive Effect of miR-34a on the FOXM1/eEF2-Kinase Axis Regulates Triple-Negative Breast Cancer Growth and Invasion. *Clin Cancer Res* 2018; 24: 4225-4241.

33 Yang Y, Ishak Gabra MB, Hanse EA, Lowman XH, Tran TQ, Li H *et al*. MiR-135 suppresses glycolysis and promotes pancreatic cancer cell adaptation to metabolic stress by targeting phosphofructokinase-1. *Nat Commun* 2019; 10: 809.

34 Xiong L, Lin XM, Nie JH, Ye HS, Liu J. Resveratrol and its Nanoparticle suppress Doxorubicin/Docetaxel-resistant anaplastic Thyroid Cancer Cells in vitro and in vivo. *Nanotheranostics* 2021; 5: 143-154.

35 Rupaimoole R, Slack FJ. MicroRNA therapeutics: towards a new era for the management of cancer and other diseases. *Nat Rev Drug Discov* 2017; 16: 203-222.

36 Ling H, Fabbri M, Calin GA. MicroRNAs and other non-coding RNAs as targets for anticancer drug development. *Nat Rev Drug Discov* 2013; 12: 847-865.

37 Ottosen S, Parsley TB, Yang L, Zeh K, van Doorn LJ, van der Veer E *et al*. In vitro antiviral activity and preclinical and clinical resistance profile of miravirsen, a novel anti-hepatitis C virus therapeutic targeting the human factor miR-122. *Antimicrob Agents Chemother* 2015; 59: 599-608.

38 van Zandwijk N, Pavlakis N, Kao SC, Linton A, Boyer MJ, Clarke S *et al*. Safety and activity of microRNA-loaded minicells in patients with recurrent malignant pleural mesothelioma: a first-in-man, phase 1, open-label, dose-escalation study. *Lancet Oncol* 2017; 18: 1386-1396.

39 Li M, Pan M, You C, Zhao F, Wu D, Guo M *et al*. MiR-7 reduces the BCSC subset by inhibiting XIST to modulate the miR-92b/Slug/ESA axis and inhibit tumor growth. *Breast Cancer Res* 2020; 22: 26.

40 Zhu H, Gan X, Jiang X, Diao S, Wu H, Hu J. ALKBH5 inhibited autophagy of epithelial ovarian cancer through miR-7 and BCL-2. *J Exp Clin Cancer Res* 2019; 38: 163.

41 Okuda H, Xing F, Pandey PR, Sharma S, Watabe M, Pai SK *et al*. miR-7 suppresses brain metastasis of breast cancer stem-like cells by modulating KLF4. *Cancer Res* 2013; 73: 1434-1444.

42 Fang Y, Xue JL, Shen Q, Chen J, Tian L. MicroRNA-7 inhibits tumor growth and metastasis by targeting the phosphoinositide 3-kinase/Akt pathway in hepatocellular carcinoma. *Hepatology* 2012; 55: 1852-1862.

43 Chang YL, Zhou PJ, Wei L, Li W, Ji Z, Fang YX *et al*. MicroRNA-7 inhibits the stemness of prostate cancer stem-like cells and tumorigenesis by repressing KLF4/PI3K/Akt/p21 pathway.

Oncotarget 2015; 6: 24017-24031.

44 Bullock AN, Fersht AR. Rescuing the function of mutant p53. *Nat Rev Cancer* 2001; 1: 68-76.

45 Thapa D, Meng P, Bedolla RG, Reddick RL, Kumar AP, Ghosh R. NQO1 suppresses NF-kappaB-p300 interaction to regulate inflammatory mediators associated with prostate tumorigenesis. *Cancer Res* 2014; 74: 5644-5655.

46 Cheteh EH, Sarne V, Ceder S, Bianchi J, Augsten M, Rundqvist H *et al*. Interleukin-6 derived from cancer-associated fibroblasts attenuates the p53 response to doxorubicin in prostate cancer cells. *Cell Death Discov* 2020; 6: 42.

47 Lin RW, Ho CJ, Chen HW, Pao YH, Chen LE, Yang MC *et al*. P53 enhances apoptosis induced by doxorubicin only under conditions of severe DNA damage. *Cell Cycle* 2018; 17: 2175-2186.

48 Sun Y, Xia P, Zhang H, Liu B, Shi Y. P53 is required for Doxorubicin-induced apoptosis via the TGF-beta signaling pathway in osteosarcoma-derived cells. *Am J Cancer Res* 2016; 6: 114-125.

49 Beltran H, Yelensky R, Frampton GM, Park K, Downing SR, MacDonald TY *et al*. Targeted next-generation sequencing of advanced prostate cancer identifies potential therapeutic targets and disease heterogeneity. *Eur Urol* 2013; 63: 920-926.

50 Hamid AA, Gray KP, Shaw G, MacConaill LE, Evan C, Bernard B *et al*. Compound Genomic Alterations of TP53, PTEN, and RB1 Tumor Suppressors in Localized and Metastatic Prostate Cancer. *Eur Urol* 2019; 76: 89-97.

51 van Dessel LF, van Riet J, Smits M, Zhu Y, Hamberg P, van der Heijden MS *et al*. The genomic landscape of metastatic castration-resistant prostate cancers reveals multiple distinct genotypes with potential clinical impact. *Nat Commun* 2019; 10: 5251.

52 Cancer Genome Atlas Research N. The Molecular Taxonomy of Primary Prostate Cancer. *Cell* 2015; 163: 1011-1025.

53 Hu J, Cao J, Topatana W, Juengpanich S, Li S, Zhang B *et al*. Targeting mutant p53 for cancer therapy: direct and indirect strategies. *J Hematol Oncol* 2021; 14: 157.

54 Vander Heiden MG, Cantley LC, Thompson CB. Understanding the Warburg effect: the metabolic requirements of cell proliferation. *Science* 2009; 324: 1029-1033.

55 Ward C, Langdon SP, Mullen P, Harris AL, Harrison DJ, Supuran CT *et al*. New strategies for targeting the hypoxic tumour microenvironment in breast cancer. *Cancer Treat Rev* 2013; 39: 171-179.

56 Lequeux A, Noman MZ, Xiao M, Van Moer K, Hasmim M, Benoit A *et al*. Targeting HIF-1 alpha

transcriptional activity drives cytotoxic immune effector cells into melanoma and improves combination immunotherapy. *Oncogene* 2021; 40: 4725-4735.

57 Reid MA, Dai Z, Locasale JW. The impact of cellular metabolism on chromatin dynamics and epigenetics. *Nat Cell Biol* 2017; 19: 1298-1306.

58 Irizarry-Caro RA, McDaniel MM, Overcast GR, Jain VG, Troutman TD, Pasare C. TLR signaling adapter BCAP regulates inflammatory to reparatory macrophage transition by promoting histone lactylation. *Proc Natl Acad Sci U S A* 2020; 117: 30628-30638.

59 Zhang D, Tang Z, Huang H, Zhou G, Cui C, Weng Y *et al*. Metabolic regulation of gene expression by histone lactylation. *Nature* 2019; 574: 575-580.

60 Wu Z, Chen H, Luo W, Zhang H, Li G, Zeng F *et al*. The Landscape of Immune Cells Infiltrating in Prostate Cancer. *Front Oncol* 2020; 10: 517637.

Figures

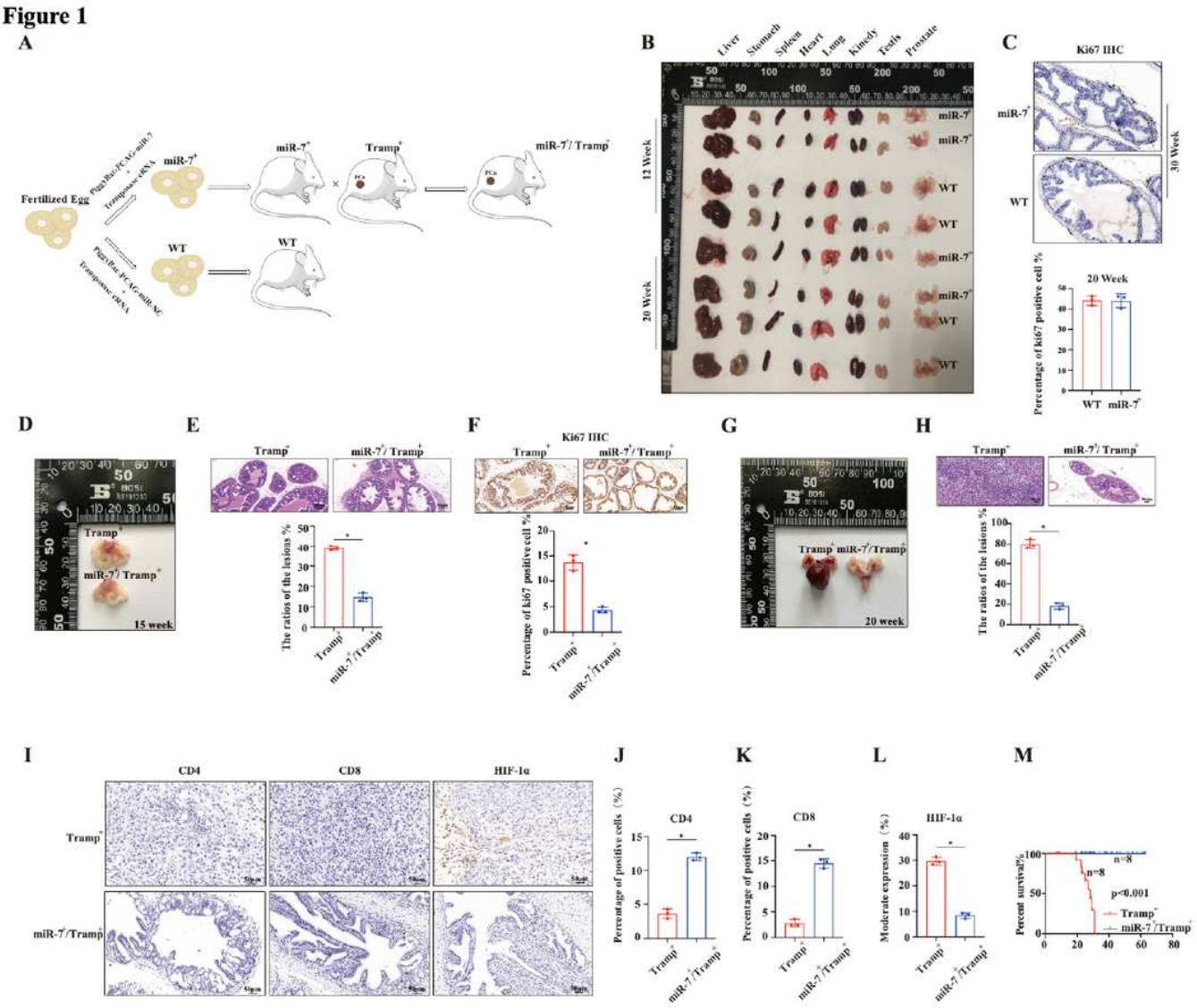

Figure 1

miR-7 expression impairs p53 null PCa development and inflames the immune microenvironment

(A) Schematic diagram for miR-7^{+} and miR-7^{+}/TRAMP^{+} mice administration.

(B) Representative images of organ development in miR-7^{+} and wild type C57BL/6 mice at 12 weeks and 20 weeks.

(C) Representative images of immunohistochemical (IHC) staining for Ki67 in resected prostate specimens. Original magnification, scale bar, 50μm.

(D, E) The anatomical structure and (D) Hematoxylin and eosin (HE) staining (E) in $TRAMP^+$ and $TRAMP^+/miR\text{-}7^+$ mice prostate specimens at 15 weeks. The ratios of prostatic intraepithelial neoplasia were calculated using Image J. Bar, the SD of experimental triplicate. Scale bar, 50μm. *$P < 0.05$.

(F) Representative images of immunohistochemical (IHC) staining for Ki-67 in resected prostate specimens. Survival analysis was performed to compare the survival conditions between $TRAMP^+$ and $TRAMP^+/miR\text{-}7^+$ mice. *$P < 0.05$. Original magnification, scale bar, 50μm..

(G, H) The anatomical structure and (G) Hematoxylin and eosin (HE) staining (H) for $TRAMP^+$ and $TRAMP^+/miR\text{-}7^+$ mice prostate at 20 weeks. The ratios of prostatic intraepithelial neoplasia were calculated using Image J. Bar, the SD of experimental triplicate. Scale bar, 50μm. *$P < 0.05$.

(I) Representative images of haematoxylin-eosin (HE) staining and immunohistochemical (IHC) staining for CD4, CD8, and HIF-1α in resected tumours. Original magnification, Scale bar, 50μm.

(J, K, L) CD4 positive cells (J), CD8 positive cells (K) and HIF-1α moderate expression cells (L) in cells from resected tumor specimens.

(M) Survival analysis was used to compare the survival condition between $TRAMP^+$ and $TRAMP^+/miR\text{-}7^+$ mice. *$P < 0.05$

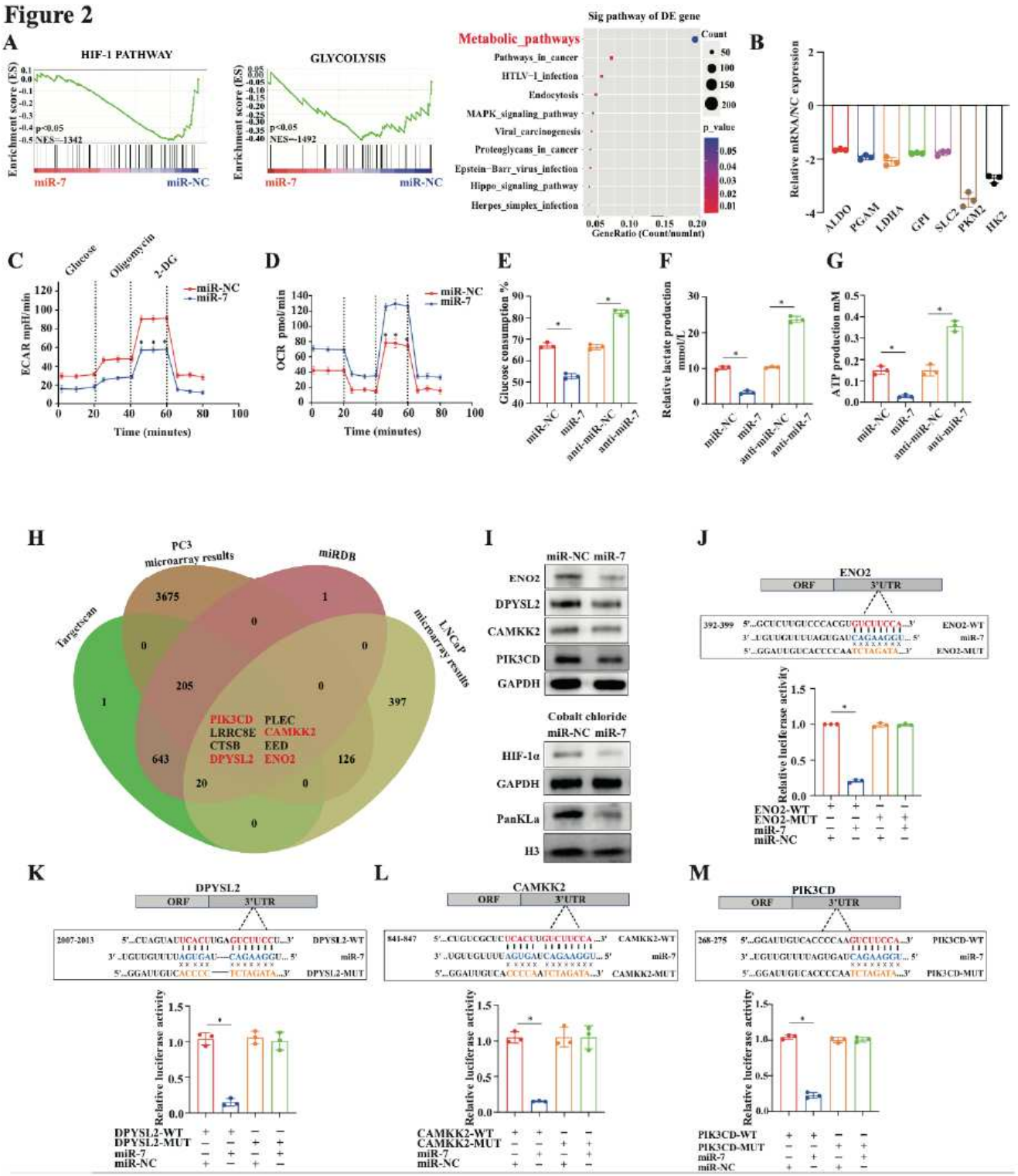

Figure 2

miR-7 regulates glucose metabolism in prostate cancer cells (PCCs)

(A) Gene set enrichment analysis (GSEA) and Gene Ontology (GO) for gene expression array data of LNCaP cells transfected with miR-NC and miR-7. GSEA plot shows the enrichment of gene signatures associated with the HIF-1, glycolysis in miR-NC and miR-7 transfected cells and GO analysis shows the

enrichment of gene signatures associated with the metabolic pathway in miR-NC and miR-7 transfected cells

(B) Quantitative real-time polymerase chain reaction (qRT-PCR) analysis for glucose metabolism-related gene expression changes in LNCaP cells after miR-7 overexpression. The level of expression was assessed using a relative ratio as compared to GAPDH. Bar, SD (SD) of experimental triplicate. *$P < 0.05$.

(C, D) Measurement of changes in the extracellular acidification rate (ECAR) and oxygen consumption rate (OCR) in LNCaP cells after miR-7 transfection. The Seahorse XF Cell Energy Phenotype Test was used to calculate the rate of ECAR and OCR. *$P < 0.05$.

(E, F and G) The measurement of glucose consumption (E), lactate levels in the culture media (F) and ATP production (G) in LNCaP cells after miR-7 transfection. Bar, SD (SD) of experimental triplicate. *$P < 0.05$.

(H) As shown in the Venn diagram (pink), 875 genes are the binding candidates of miR-7 according to the prediction using miRDB. The Venn diagram (green) also shows that 556 genes are the putative targets of miR-7 according to Targetscan prediction. Furthermore, the Venn diagram (yellow) shows that 3687 genes are significantly downregulated in LNCaP cells. The Venn diagram (orange) shows that 4012 genes are significantly downregulated in PC3 cells transfection with miR-7. PIK3CD, CAMKK2, DPYSL2, and ENO2 are the targets of miR-7.

(I) Western blot analysis for protein levels of ENO2, DPYSL2, CAMKK2, PIK3CD, HIF-1α, and PanKLa in LNCaP cells transfected with miR-7 or miR-NC.

(J) Predicted binding sites of miR-7 within the 3'-UTR of ENO2 (ENO2-wild type (WT)) or mutant (MUT) variants (ENO2-MUT). LNCaP cells were co-transfected with GV208 dual-luciferase vectors cof ENO2-WT or ENO2-MUT and miR-NC or miR-7. Bar, SD (SD) of experimental triplicate. *$P < 0.05$.

(K) Predicted binding sites of miR-7 within the 3'-UTR of DPYSL2 (DPYSL2-wild type (WT)) or mutant (MUT) variants (DPYSL2-MUT). LNCaP cells were co-transfected with GV208 dual-luciferase vectors of DPYSL2-WT or DPYSL2-MUT and miR-NC or miR-7. Bar, SD (SD) of experimental triplicate. *$P < 0.05$.

(L) Predicted binding sites of miR-7 within the 3'-UTR of CAMKK2 (CAMKK2-wild type (WT)) or mutant (MUT) variants (CAMKK2-MUT). LNCaP cells were co-transfected with GV208 dual-luciferase vectors of CAMKK2-WT or CAMKK2-MUT and miR-NC or miR-7. Bar, SD (SD) of experimental triplicate. *$P < 0.05$.

(M) Predicted binding sites of miR-7 within the 3'-UTR of PIK3CD (PIK3CD -wild type (WT)) or mutant (MUT) variants (PIK3CD-MUT). LNCaP cells were co-transfected with GV208 dual-luciferase vectors of PIK3CD-WT or PIK3CD-MUT and miR-NC or miR-7. Bar, SD (SD) of experimental triplicate. *$P < 0.05$.

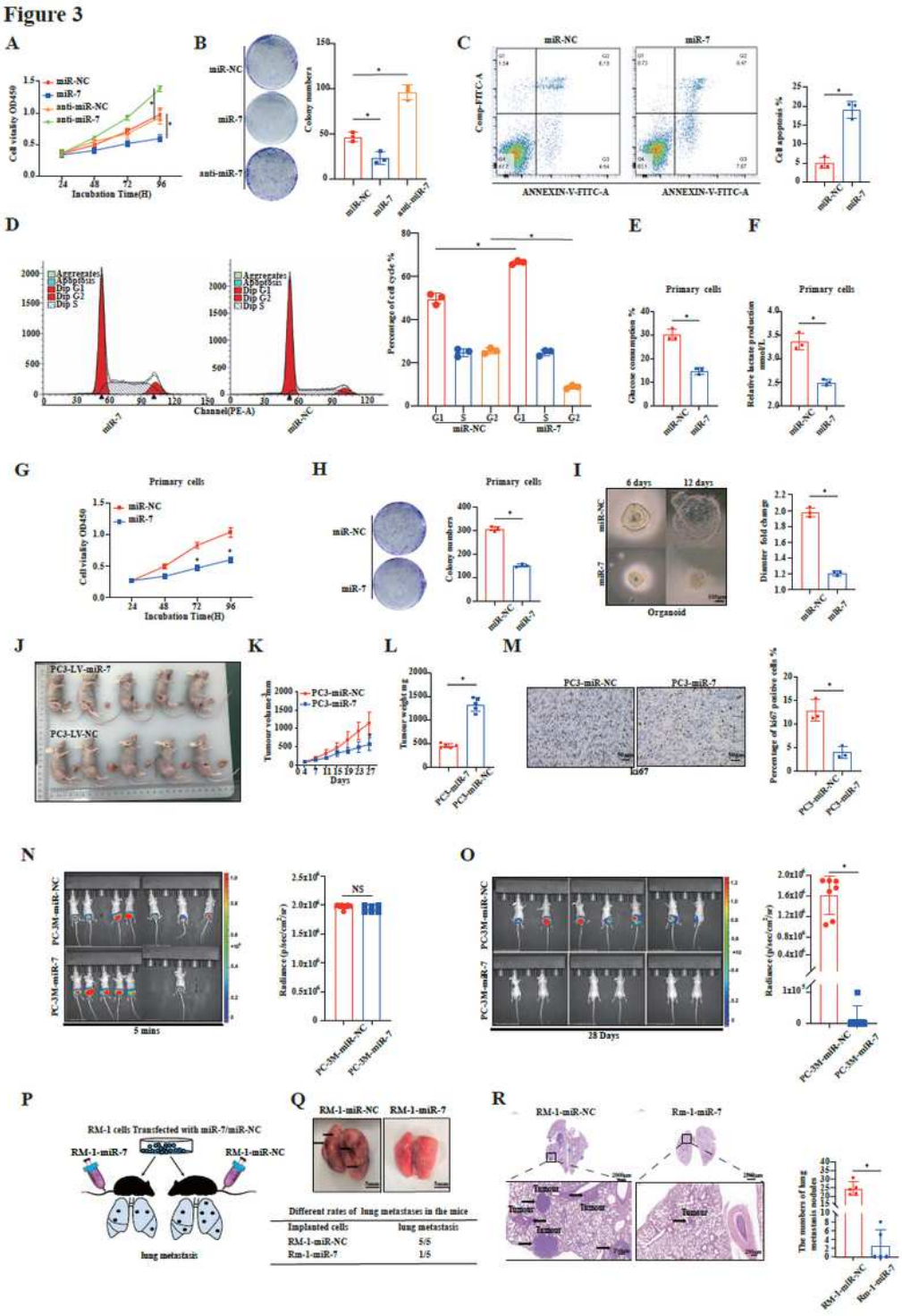

Figure 3

miR-7 inhibites proliferation, colony formation, migration, and invasion of PCa cells in vitro and in vivo.

(A) Cell proliferation assay in LNCaP cells after abnormal miR-7 expression. Bar, SD of experimental triplicate. *$P < 0.05$.

(B) Cell colony formation assay in LNCaP cells after abnormal miR-7 expression. Bar, SD of experimental triplicate. *$P < 0.05$.

(C) Cell apoptosis percentage in LNCaP cells after miR-7 transfection assessed by flow cytometry (FCM). Bar, SD of experimental triplicate. *$P < 0.05$.

(D) Cell cycle analysis in LNCaP cells after miR-7 transfection assessed by FCM. Bar, SD of experimental triplicate. *$P < 0.05$.

(E, F) The measurement of glucose consumption (E) and lactate levels in the culture media (F) of primary prostate cancer (PCa) cells after miR-7 transfection. Bar, SD of experimental triplicate. *$P < 0.05$.

(G) Cell proliferation assay for the primary PCa cell line after miR-7 transfection. Bar, SD of the experimental triplicate. *$P < 0.05$.

(H) Cell colony formation assay for the primary PCa cell line after miR-7 transfection. Bar, SD of experimental triplicate. *$P < 0.05$.

(I) Organoid growth was evaluated by assessing the change in relative diameter after miR-7 transfection. Bar, SD of experimental triplicate. Scale bar, 100μm. *$P < 0.05$.

(J) Representative images of tumor-bearing nude mice and resected tumors 27 days after injection of PC3 cells stably expressing miR-7.

(K) Tumor growth curves for xenografted mice models injected subcutaneously with PC3 cells transfected with miR-NC or miR-7 (n = 5 in each group). The tumor volume was calculated using the following formula: $(\text{shortest diameter})^2 * (\text{longest diameter}) * 0.5$. Bar, SD for 5 mice. *$P < 0.05$.

(L) Weights of the resected tumors between miR-NC or miR-7. Bar, SD for 5 mice. *$P < 0.05$.

(M) Representative images of IHC staining for $Ki\text{-}67^+$ cells in resected tumors. Original magnification, scale bar, 50μm. *$P < 0.05$.

(N, O) Representative bioluminescence images of prostate specimens inoculated with luciferase-labeled PC-3M cells transfected with miR-NC or miR-7 in male nude mice after injection (N) and at day 27 (O). Bar, SD for 6 mice. *$P < 0.05$.

(P) The metastatic model schematic diagram. Lung metastasis was induced by tail vein injection of RM-1 cells transfected with miR-NC or miR-7 (n = 6 in each group).

(Q) Representative images for metastatic seeding and growth in explanted lungs. Black arrows indicate metastatic lesions. Different numbers of lung metastasis nodules between the miR-NC group and miR-7 group (P). *$P < 0.05$. Scale bar, 5mm.

(R) Representative images for HE staining show the differences in the number of lung metastasis events between the miR-NC and miR-7 groups. Scale bar, 2000μm and 200μm.

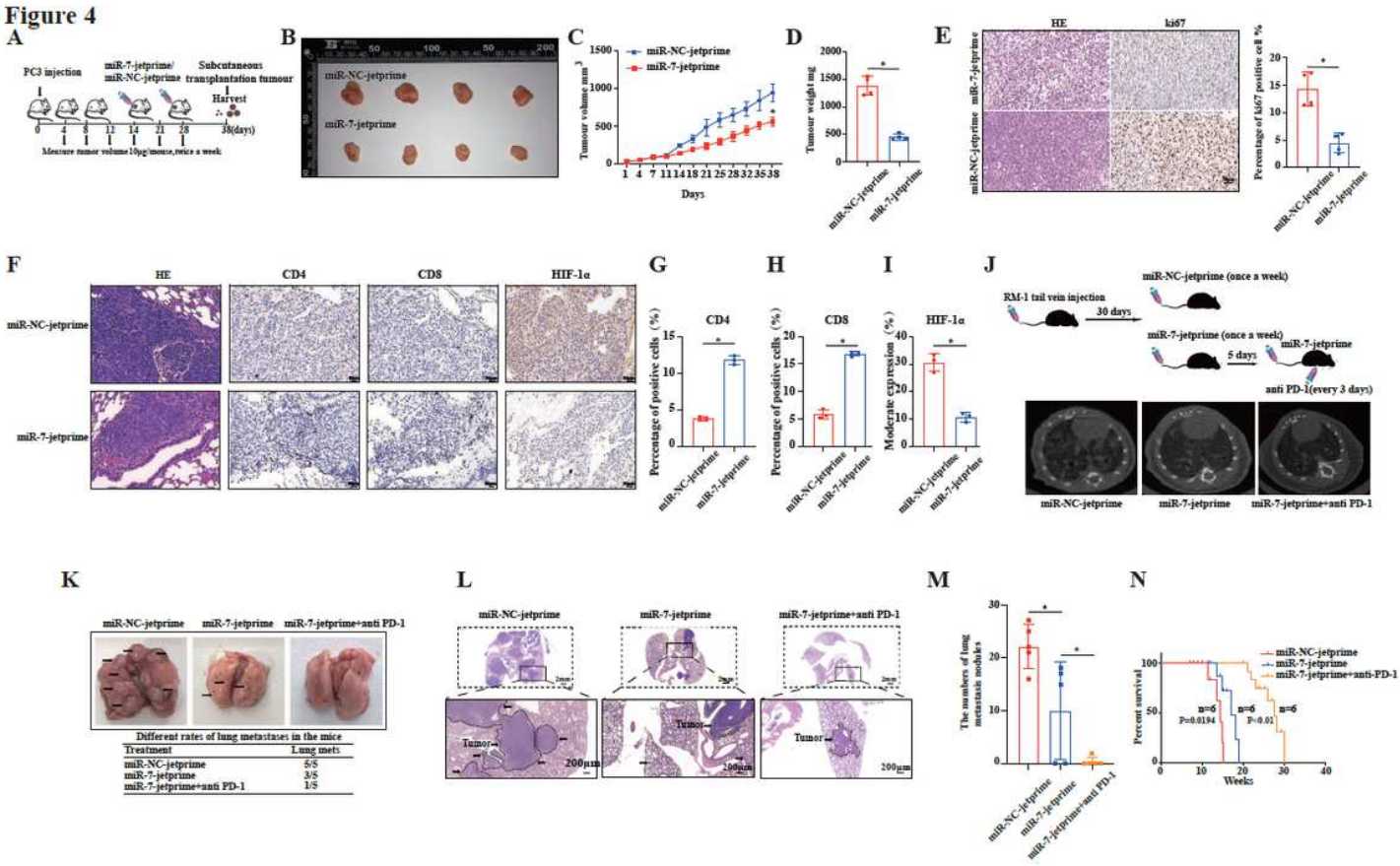

Figure 4

Administration of vivo-jetprime-miR-7 impairs the growth of PCa xenografts and lung metastasis in vivo

(A) Schematic diagram for vivo-jetprime-miR-7 administration. After two weeks of subcutaneous tumor formation in a mouse model of PCa, jetprime-miR-7 or jetprime-miR-NC was injected intratumorally twice every 7 days, 10μg each time, for a total of three weeks, and the tumor mass and volume were measured after one week of its formation (n = 4 in each group).

(B) Representative images of the resected tumors at day 38 (n = 4 in each group).

(C) Tumor growth curves for xenografted mouse models after jetprime-miR-7/jetprime-miR-NC injection. The tumor volume was calculated using the following formula: (shortest diameter)^2 * (longest diameter) *0.5. Bar, SD for 4 mice. *P < 0.05.

(D) Weights of the resected tumors between the two groups. Bar, SD for 4 mice. *P < 0.05.

(E) Representative images for HE staining and IHC staining for Ki-67 in resected tumors. Original magnification, scale bar, 50μm.

(F) Representative images of HE staining and IHC staining for CD4, CD8, and HIF-1α in resected tumors. Original magnification, scale bar, 50μm.

(G, H, I) CD4 positive cells (G), CD8 positive cells (H), and HIF-1α moderate expression in cells (I) of resected tumors.

(J) Representative images of computed tomography (CT) examination after the tail vein injection of jetprime-miR-7, jetprime-miR-NC or jetprime-miR-7+anti-PD-L1 for four times (once a week).

(K) Representative images of metastatic seeding and growth in explanted lungs after the tail vein injection of jetprime-miR-7, jetprime-miR-NC, or jetprime-miR-7+anti-PD-L1 for four times. Black arrows indicate metastatic lesions. Scale bar, 5 mm.

(L) Representative images of HE staining for the differences in the number of lung metastasis events among jetprime-miR-7, jetprime-miR-NC, or jetprime-miR-7+anti-PD-L1 group. Scale bar, 2000μm or 200μm.

(M) Differences in the lung metastasis nodules among jetprime-miR-7, jetprime-miR-NC, or jetprime-miR-7+anti-PD-L1 group. *$P < 0.05$.

(N) Survival analysis was used to compare the survival conditions among the jetprime-miR-7, jetprime-miR-NC or jetprime-miR-7+anti-PD-L1 group. *$P < 0.05$.

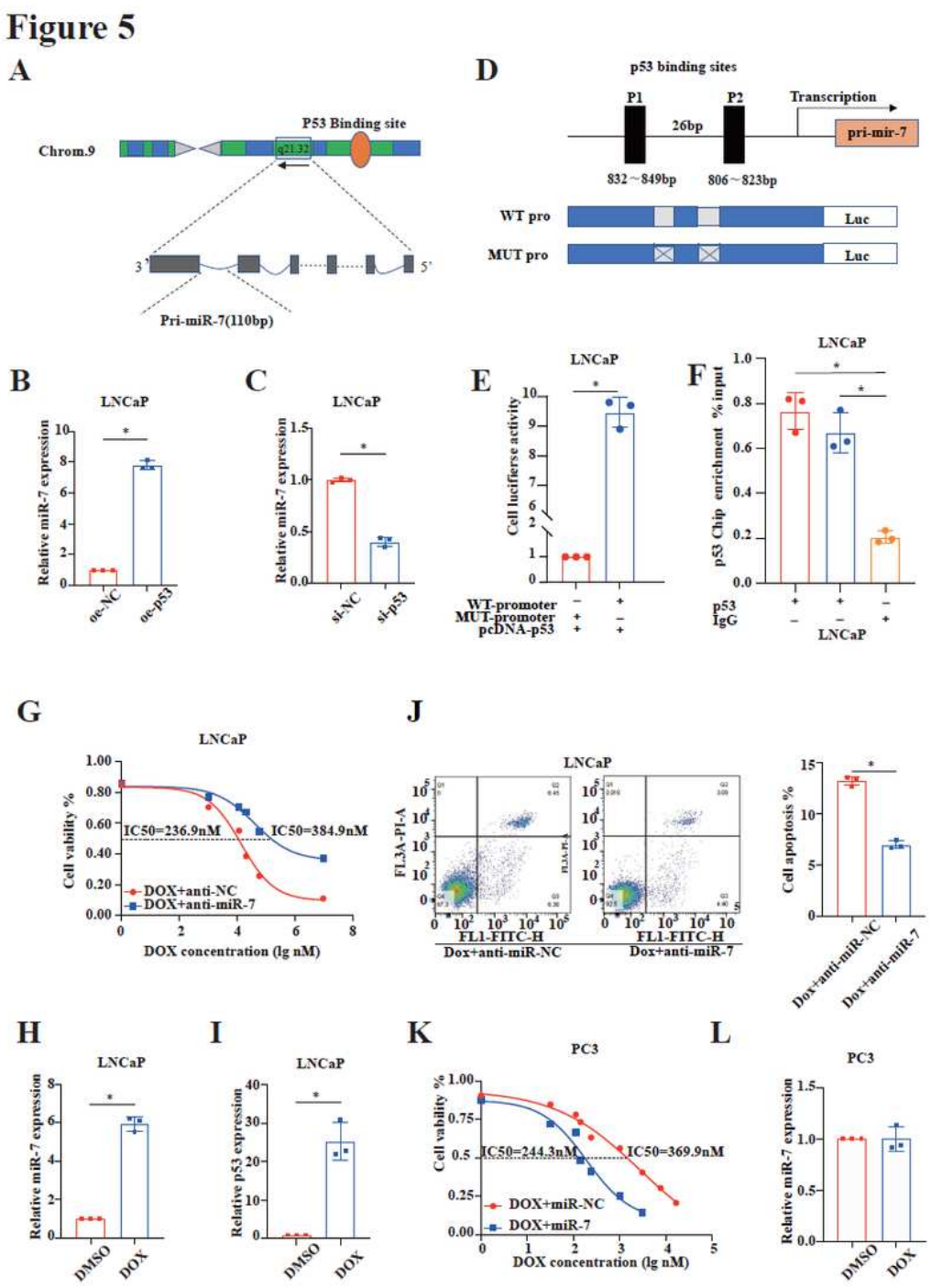

Figure 5

p53 transcriptionally upregulates miR-7 expression

(A) The genomic location of p53 and pri-miR-7-1 genes.

(B, C) qRT-PCR analysis of miR-7 and p53 mRNA in LNCaP cells 48 h after transfection with p53 overexpression plasmids/ short interfering (si) RNA (si-p53, 20μM) constructs. The expressions of miR-7 and p53 were assessed using a relative ratio with that of (si) RNA (si-NC) transfected cells. The transfection efficiency was verified by western blotting. Bar, SD of experimental triplicate. *$P < 0.05$.

(D, E) Luciferase reporter assay. LNCaP cells were transfected with reporter plasmid vectors, containing the wild-type (WT) or mutant (MUT) seed sequences of p53 binding sites, in the pri-miR-7-1 promoter region and pcDNA-p53. Bar, SD of experimental triplicate. *$P < 0.05$.

(F) Relative chromatin immunoprecipitation enrichment values in the indicated regions of the p53 binding sites are expressed as percentages relative to the input DNA. Bar, SD of experimental triplicate. *$P < 0.05$.

(G, K) The half maximal inhibitory concentration (IC50) of doxorubicin (Dox)+anti-miR-NC/Dox+anti-miR-7 treatment (48 h) in LNCaP cells (G), and IC50 of Dox+miR-NC/Dox+miR-7 mimics in PC3 cells (K).

(H, I) qRT-PCR shows changes in p53 and miR-7 mRNA expression upon Dox treatment (48 h). The expression of miR-7 (H) and p53 (I) was assessed using a relative ratio with dimethyl sulfoxide (DMSO) treatment in LNCaP cells. Bar, SD of the experimental triplicate. *$P < 0.05$.

(J) Cell apoptosis percentage assessed by FCM in LNCaP cells after Dox+anti-miR-7/Dox+anti-miR-NC treatment (48 h). Bar, SD of experimental triplicate. *$P < 0.05$.

(L) The expression of miR-7 was assessed using a relative ratio with that of negative control (NC) vector or DMSO treatment in PC3 cells. Bar, SD of experimental triplicate. *$P < 0.05$.

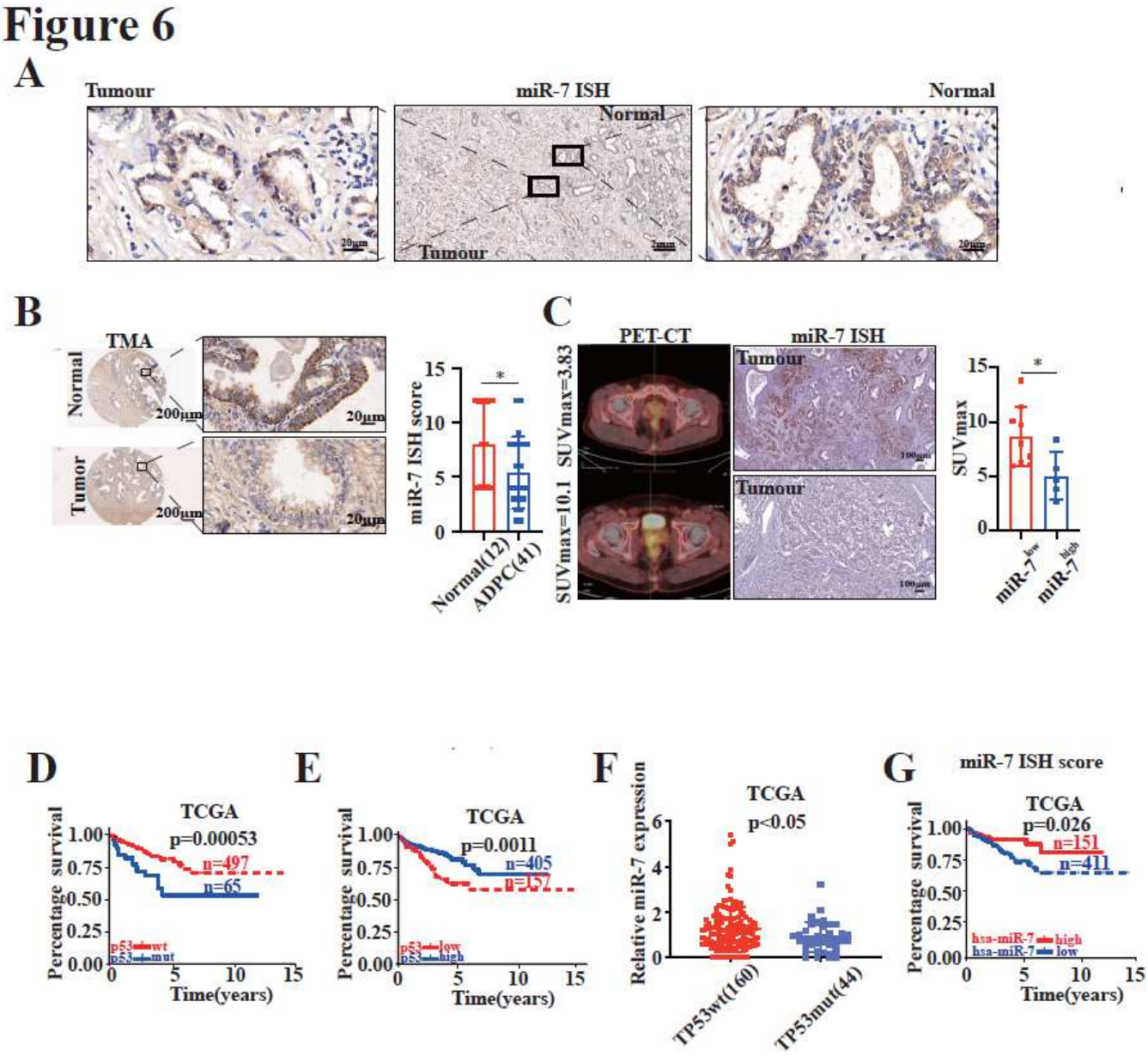

Figure 6

Database analyses for miR-7 and p53 expressions in PCa

(A) In situ hybridization (ISH) results for miR-7 in PCa tumor- and para cancerous tissues; scale bar, 2000μm or 20μm.

(B) Tumor microarray analysis between miR-7 in PCa tumor tissues (n = 41) and normal tissues (n = 12). Scale bar, 200μm or 20μm. *$P < 0.05$.

(C) Correlation between ISH score and SUVmax in patients with PCa who underwent PET-CT scanning (n = 14). Scale bar, 100μm. *$P < 0.05$.

(D) Kaplan-Meier analysis reveals overall survival in patients with PCa (n = 562) based on the differential expression of p53. * P =0.00053.

(E) Kaplan-Meier analysis reveals overall survival in patients with PCa (n = 562) based on the relative expression of p53. * P =0.0011.

(F) Analysis of miR-7 expression in patients with PCa carrying p53 mutations (n = 44) as compared to those with p53 wild type (WT) (n = 160) using The Cancer Genome Atlas (TCGA) database. *$P < 0.05$.

(G) Kaplan-Meier analysis reveals the overall survival in patients with PCa (n = 562) based on the relative expression of miR-7. * P =0.026.

Supplementary Files

This is a list of supplementary files associated with this preprint. Click to download.

- SupplementaryFigure.pdf
- Table.docx